Visualising nascent chain dynamics at the ribosome exit tunnel by cryo-electron microscopy

Abid Javed[1,✉], Anaïs .M.E. Cassaignau[2,✉], Tomasz Wlodarski[2,✉], Lisa D. Cabrita[2,✉], John Christodoulou[2,✉], and Elena V. Orlova[1,✉]

[1]Institute of Structural and Molecular Biology, Birkbeck College, Malet Street, London WC1E 7HX, United Kingdom.
[2]Institute of Structural and Molecular Biology, University College London, Gower Street, London WC1E 6BT, United Kingdom.

One of the important questions in protein synthesis on the ribosome is how the nascent polypeptide chains fold during translation. Addressing this question has strong implications to health and disease. Ribosomes play an essential role in maintaining a healthy cellular proteome by modulating co-translational folding. And folding of the nascent chain (NC) is likely to be initiated within the ribosomal exit tunnel. Here, we report high-resolution cryo-EM structures of stalled ribosome nascent-chain complexes (RNCs) at two biosynthetic translation time-points that examine the role of the ribosome during co-translational folding. Structures of the RNCs reveal that NC is highly dynamic and adopts a range of trajectories within the vestibule of the exit tunnel, affecting positions of the folded immunoglobulin domain outside the ribosome. Local rearrangements of several ribosomal components suggest key sensor checkpoints that monitor co-translational protein folding.

ribosome | nascent chain | co-translational folding | cryo-EM

Correspondence: ***j.christodoulou@ucl.ac.uk***
e.orlova@mail.cryst.bbk.ac.uk

Introduction

Ribosomes are nano-machines that translate information coded in a messenger RNA into proteins in all living organisms. Recently, it has been found that ribosomes can also play a significant role in the process of co-translational folding by modulating the folding of a nascent chain (NC) during translation (Kaiser et al., 2011; Cabrita et al., 2016; Javed et al., 2017; Samulson et al., 2018; Liu et al., 2019). Nascent chains (NC) can begin to acquire secondary structural elements in a co-translational manner during emergence via the ribosome exit tunnel within the large subunit of the ribosome (Netzer W. et al., 1997; Thommen et al., 2017). Studies by cryo-EM have shown NC folding within the exit tunnel is largely limited to formation of rudimentary secondary structure, predominantly α helices within different areas of the tunnel while β hairpins as well as the formation of small domains in the wider vestibule region of the tunnel (Kosolapov and Deutsch., 2009; Bhushan et al., 2011; Lu et al., 2011; Nilsson et al., 2015; Holtkamp et al., 2015; Nilsson et al., 2017; 2017; Su et al., 2017; Agirrezabala et al., 2017; Tian et al., 2018). Nonetheless, the polypeptides with more complex tertiary structure fold close to and outside the tunnel, as found for spectrin - a three-helix bundle protein, and titin, an all beta-sheet immunoglobulin domain (Nilsson et al., 2017; Tian et al., 2018). Biochemical and biophysical studies using FRET and PEGylation support these observations (Holtkemp et al., 2015; Kosolapov and Deutsch 2010). NCs studies by cryo-EM provided us with snapshots of some states of the NCs within the ribosomal tunnel. These results revealed structural details regarding stalling, folding of NC and details on how the ribosome and NC co-ordinate activities in the upper and central tunnel (Bhushan et al., 2011; Nilsson et al., 2015; Agirrezabala et al., 2017, Su et al., 2017). Yet, how biochemical and physical properties of the ribosome tunnel vestibule, i.e. the lower tunnel, affect the position of the NC and therefore the process of folding is poorly understood, largely due to the flexibility of the NC in this widest region of the tunnel.

NCs comprising the fifth and sixth domains of ABP-120 filamin protein (referred below as FLN5 and FLN6) have been analysed by NMR in the vicinity of the ribosome (Hsu et al., 2007;2009; Cabrita et al., 2009). In these ribosome-NC complexes (RNCs), the FLN5 domain is tethered to the ribosome via different length sequences from FLN6 domain (Figure 1a). Initial analyses of these RNCs revealed the transition of FLN5 to the folded state occurs when it is bound to the ribosome by a linker of approximately 45 amino acids (Cabrita et. al., 2016; Cassaignau et al., 2016). Details on the structural organisation of FLN5 and FLN6 NC within the ribosome and the effect of the ribosome on the folding of FLN5 remains

to be understood that would help to address the question on how the ribosome modulates co-translational protein folding.

In this study, we report cryo-EM structures of SecM stalled FLN5-45 and FLN5-47 RNCs, where FLN5 is tethered to the ribosome by 45 and 47 amino acids using sequence from FLN6 and SecM (Figure 1a). Statistical analysis of cryo images allowed us to obtain a set of structures reflecting the most representative populations of RNCs at two points of translation. We have found that the NCs are dynamic within the tunnel and can adopt a variety of NC trajectories within the tunnel vestibule, resulting in distinct conformations for each NC linker within the exit tunnel, and three most probable positions of folded FLN5 NC. Trajectories adopted by the NC reveal the dynamic process of co-translational folding of the NC on the ribosome and in particular how interactions with the ribosome's tunnel surface likely contribute to the productive folding of an emerging NC inside a cell.

Results

Overall organisation of RNC complexes

Two FLN5-RNCs were chosen as representative biosynthetic snapshots of FLN5 NC (residues 646 to 750), which is tethered to the ribosome by 45 or 47 amino acids. The tether comprises either 26 (aa 751 to 776) or 28 (aa 751 to 778) N-terminal amino acids from FLN6, together with the 17 amino acid SecM stalling sequence (Nakatogawa and Ito, 2001) (Figure 1a). Data for FLN5-45 and FLN5-47 RNCs were collected on a Titan Krios electron microscope (Thermo Fisher ScientificTM), operating at 300 kV and equipped with K2 Summit direct electron detector (see Methods; Table 3). We used RELION 2 for structural analysis to identify different conformational states of the RNCs (see Methods, Supplementary Figure 1). Local resolution maps of FLN5-45 and FLN5-47 RNC structures exhibited both stable and flexible regions in both the ribosome and NC (Supplementary Figure 2). In the structures obtained, the two ribosomal subunits have an average resolution of ~ 3.5 Å. The resolution of NC within the tunnel was lower compared to the overall resolution of the ribosome, indicating a higher level of flexibility in the FLN6 NC linker (Supplementary Figure 2). The 3D classification enabled us to distinguish structures according to the FLN6 linker positions within the ribosome tunnel vestibule (Figure 1b, c; see Methods, Supplementary Figure 1). Overall, these structures enabled us to derive the most significant pathways adopted by the NC within both RNC complexes.

The RNC complexes analysed by cryo-EM were in the SecM-arrested state and show well-established features including the P-site tRNA, located in the peptidyl transferase centre (PTC), between the small and large ribosomal subunits and linked to the NC at the entrance to the exit tunnel (Figure 1b). The NC density spans the entire ~ 100 Å length of the exit tunnel on the 50S and can be sub-divided into three major regions depending on the distance from PTC (Figure 1b): upper - between the entrance and the tunnel constriction formed by uL4 and uL22; central - from the tunnel constriction site up to the A1321 nucleotide of H50 (starting at ~ 45 Å from the tunnel entrance); and the vestibule region (starting at ~ 70 Å from the top) (Figure 1b). The P-site tRNA (shown in blue, Figure 1) is attached to the NC via the Gly165 residue, which is the penultimate residue observed in the SecM sequence at the entrance to the tunnel. Density corresponding to the SecM sequence of the NC is well defined and threads throughout the upper tunnel part, which is ~ 10 Å wide. The density within the central part of the tunnel was assigned to FLN6 sequence. For each RNC, the resolution was sufficient to model side chains of residues 776-773 (FLN5-45) and 778-774 (FLN5-47) in FLN6 (Figure 2). The remaining 22 (FLN5-45) and 24 (FLN5-47) residues were traced as poly-alanine chains within the tunnel vestibule. This enabled us to model three most plausible NC trajectories adopted within the vestibule region of ~ 25 Å wide (Table 1). Close to the tunnel exit and in the proximity to the ribosome surface, the FLN5 domain tethered to FLN6 was seen as a bulk of density in both FLN5-45 and FLN5-47 RNCs. Fitting of the crystal structure of FLN5 domain (McCoy et al., 1999) shows the volume of these densities is consistent with the globular conformation of FLN5 (Table 2; Figure 1c; Supplementary figure 7).

Three NC pathways were differentiated according to the identified NC trajectories within the vestibule, referred further as "states" (1 to 3) for each RNC length. State 1 corresponds to a population of NCs where FLN6 is in close proximity to H24 of the 23S rRNA in the vestibule, state 2 represents NC that is positioned between H24 and H7 23S rRNA, and state 3 corresponds to FLN6 NC located close to H7 23S rRNA; the relative populations of the observed FLN5-45 and FLN5-47 states in the cryo-EM datasets are shown in Table 1, (Figures 1b, c). Each of the states observed was accompanied by small local changes in the ribosomal elements lining the vestibule (see below). Analysis of both complexes showed that state 2 was represented by a large number of particles (Table 1), which is likely the most character-

istic (meta-stable) conformation of the NC at the corresponding linker length during biosynthesis.

Location of SecM and its interactions with the tunnel

Each of the structures of the FLN5-RNCs show well defined density within the upper and first half of the central tunnel region corresponding to the SecM NC (Gly165 - Phe150) (Figure 2a). Modelling of SecM NC interactions with ribosome tunnel elements was done using NC states 2, where SecM was resolved on average at ~ 5 Å. These models were subsequently used to trace SecM in less populated states in both RNCs. SecM NC was traced in the same position within the upper tunnel in all RNC states (Figure 1c). The SecM models enabled us to reveal major site-specific SecM interactions with the ribosomal exit tunnel that induce translational arrest, as established by previous studies (Nakatogawa and Ito, 2001; Bhushan et al., 2011; Zhang et al., 2015) (Figure 2b; Supplementary Figure 3). The point of interaction between Arg163 of SecM and nucleotides U2506 and A2451 (Int163,2506) of 23S rRNA at the PTC in both FLN5-45 and FLN5-47 RNC complexes was identified (Figure 2b; Supplementary Figure 3). Close to the PTC in the upper tunnel, SecM Gln160 appears to interact with A2062 in FLN5-45 RNC (Figure 2b; Supplementary Figure 3).Another interaction is found between Trp155 (SecM) and A751 (23S rRNA) (Int155,751), located close to the uL4-uL22 constriction site and is visible in structures of both complexes of FLN5-45 and FLN5-47 RNC (Figure 2b; Supplementary Figure 3). The NC density corresponding to the pi-stacking interaction Int155,751 in the structure is in a good agreement with previous structural and mutagenesis studies reporting that Trp155 to Ala155 mutation reduces SecM stalling (Nakatogawa and Ito 2002, Bhushan et al., 2011 and Zhang et al., 2015) (Figure 2b; Supplementary Figure 3).

To analyse changes in SecM conformation within the upper tunnel between the NC states, we measured the distances between Int163,2506 and Int155,751 of SecM (~ 20 to 22Å), which is shorter than the expected ~ 30 Å distance for an extended SecM NC chain of the same length (assuming that the distance between two residues in an extended chain is ~ 3.4 Å) (Supplementary Figure 4a). This indicated a more compact form of SecM observed in FLN5 RNCs, which is consistent with former studies suggesting the compaction of the chain (Supplementary Figure 4a) (Woolhead et al., 2004, Gumbart et al., 2012; Zhang et al., 2015). The compaction likely is a feature of SecM NC to induce site-specific ribosome stalling. Moving towards the tunnel constriction we have found that the N terminal residues (Pro153–Ser151) of the SecM backbone (main chain) undergo lateral shifts of ~ 3.8 Å between states 2 of FLN5-45 and FLN5-47 (Supplementary Figure 4b). This shift of the polypeptide chain is possibly related to the residue Pro153 of SecM, mutation of which was recently shown to make SecM more flexible within the tunnel (Bracken and Woolhead, 2019), hence identifying this point in SecM NC to play some role in SecM activity within the ribosome exit tunnel. This flexibility of SecM was also predicted by molecular dynamics simulation of SecM NC within the tunnel (Gumbart et al., 2012), suggesting to us that the shift observed in our SecM NC structures around the tunnel constriction possibly correlates with the NC flexibility downstream in the vestibule. Altogether, the key interactions identified in our structures confirm previously described structures of SecM-arrested RNCs (Bhushan et al., 2011; Zhang et al., 2015) and suggest that SecM globally is fixed enough within the tunnel in FLN5-RNC structures to interact with the tunnel and stall ribosomes during translation.

Conformations of the FLN6 linker within the central part of the tunnel

The central tunnel region located beyond the tunnel constriction site formed by uL4 and uL22 is slightly wider and has a diameter of ~ 15 Å. (Figures 1b). It is lined with nucleotides of 23S rRNA domains H22, H23, H50 and uL22, uL23 ribosomal protein segments (Figure 1b). The structures of the FLN5-45 and FLN5-47 RNCs show NC density along the entire central tunnel region at a resolution of ~ 6.0 Å (Figure 2c; Supplementary Figure 2) allowing us to trace the FLN6 polypeptide chain. All states of FLN6 NC at both linkers show that EM densities of the NC have similar positions within the central tunnel, but vary in local interactions with the central tunnel elements (Figure 1c). In the RNCs, the central tunnel accommodates about 10 residues of FLN6 NC, from which four residues of the C-terminal FLN6 NC and two residues from the cloning vector are modelled (Leu-773 to Glu-778: FLN5-45 and residues Leu-773 to Lys-778: FLN5-47; see methods, Figure 2b). The modelling of these six residues was performed on the structures corresponding to states 2, while the remaining part of the NC was modelled as a poly-alanine chain. The fitted models were used for interpretation of FLN6 NC behaviour within the central and vestibule regions of the tunnel in both FLN5-45 and FLN5-47 RNCs.

It was found that a two-amino acid difference in sequence and length of FLN6 linker between FLN5-45 and

FLN5-47 RNCs plays a role in changes within NC interactions, affecting NC dynamics and hence folding of the FLN5 domain (Figure 2c). Comparison of state 2 structures shows that the FLN6 NC makes several contacts with the ribosome protein uL22 at the central tunnel region (Figure 2c). In FLN5-45 RNC, FLN6 appears to interact with Arg84 of uL22 via Glu-778 (FLN6) (Figure 2c – upper panel). At the same position in the tunnel in FLN5-47, Thr-776 of FLN6 NC interacts with uL22 (Arg84) (Figure 2c – bottom panel). The nature of these interactions appears to be non-specific. Published structures of NCs of different sequences also show NC interaction with Arg84 of uL22 (Agirrezabala et al., 2017; Su et al., 2017), indicating that uL22 acts as a key and non-discriminatory interaction point between the ribosome tunnel and the NC, in our case with FLN6 NC in FLN5 RNCs.

The lower tunnel region (at entrance to the tunnel vestibule), occupied by A1321 nucleotide of H50 23S rRNA and the beta-hairpin loop of uL23 (Figure 1b) shows variations in contact points made by FLN6 NC between FLN5-45 and FLN5-47 RNCs (Supplementary figure 5). This is clearly evident in NC states 2 of FLN5-45 and FLN5-47 RNC and state 3 of FLN5-47 RNC (Supplementary figure 5). In state 2 of FLN5-45 RNC, FLN6 NC interacts with both A1321 nucleotide and uL23 (Supplementary Figure 5a). In state 2 of FLN5-47 RNC, only one contact is observed between A1321 nucleotide and NC (Supplementary Figure 5b). Interestingly, state 3 of FLN5-47 RNC shows two contacts of NC with H50 and uL23, similar to state 2 FLN6 of FLN5-45 RNC (Supplementary Figure 5c). At this region of the tunnel in both RNCs, the sequence of FLN6 NC corresponds to multiple lysine residues (Supplementary figure 5), indicating this interaction is possibly mediated by electrostatics of both the NC and the ribosome tunnel. Overall, it appears that the strength of uL23-H50 rRNA interaction with NC plays a role in determining the trajectory of the NC at the vestibule, shifting it either towards H7 (state 3) or exiting via the middle of the tunnel (state 2 - Figure 3).

Trajectories of NC within the tunnel vestibule

The vestibule is the widest region of the exit tunnel, with an average diameter of ~ 22 Å (Figure 1b). The ribosome tunnel vestibule is lined by negatively charged 23S rRNA (nucleotides of H50, H24, H7 and H4) and loops with positively charged residues from uL23, uL24 and uL29 proteins (Figure 1b). The large diameter of the vestibule permits greater flexibility to the NC, as observed in the different RNC states (Figure 1; Table 1). The resolution of the FLN6 NC in the vestibule was ~ 8.0 Å, sufficient to trace the N-terminal portion of FLN6 NC as polyalanine chain (from residue Lys771 onwards towards the C-terminal Ala751) (Figure 3). A point of bifurcation of FLN6 NC trajectories was found at A1321 nucleotide of H50 (23S rRNA), positioned at the start of the tunnel vestibule (Figure 3). It is likely that several positively charged residues in FLN6 NC sequence located at the vestibule (i.e. Lys771-Lys770-Lys768) make some electrostatic interactions with negatively charged 23S rRNA (Figure 3a; Supplementary Figure 5). These non-specific charge-mediated interactions give rise to multiple NC positions along the tunnel vestibule, enabling the identification of three main states in both RNCs: one is in close proximity to the H24 rRNA domain (state 1), the second at the centre of the vestibule (state 2) and the last one being close to the H7 rRNA domain (state 3) (Figure 3).

The N-terminal region (from residues Ala767 onwards) of FLN6 NC in states 1 in both FLN5-45 and FLN5-47 RNCs interacts with nucleotides of H50 and H24 domains of 23S rRNA and uL24 loop (Figure 3 and b respectively). Interestingly, FLN5-45 NC state 1 shows a bulk of density, attached to nucleotides H50-H24 of 23S rRNA and likely relates to a compaction of FLN6 NC (Figure 3a; Supplementary Figure 7b). This short-lived NC state represents a snapshot of a possible conformation adopted by FLN6 NC in FLN5-45 RNC. State 3 of FLN6 NC in both FLN5-45 and FLN5-47 RNCs shows the NC making several contacts with uL23 and uL29 loop as well as the nucleotides of H4 and H7 domains of 23S rRNA (Figure 3a and 3b).

It was demonstrated that uL23, uL24 and uL29 could be cross-linked with emerging NCs, indicating that these proteins can actively interact with an emerging NC within the tunnel vestibule (Peterson et al, 2010). Our RNC structures of different NC states demonstrated variability in positions of ribosome tunnel uL23, uL29 and uL24 proteins by ~ 2 to 5 Å (Figure 4). For instance, comparison of ribosome states 2 of FLN5-RNCs shows uL23 movement of ~ 3 Å between FLN5-45 and FLN5-47 RNCs (Figure 4a). uL29 loop has the smallest shift in states 2 between FLN5-45 and FLN5-47 of ~ 1 Å (Figure 4b). For uL24, the loop moves by ~ 5 Å between states 2 of FLN5-45 and FLN5-47 RNCs (Figure 4c). Interestingly, cross-comparison of uL24 tunnel loop shows that it undergoes a shift of ~ 3 to 4 Å between states 1, 2 and 3 for each RNC reported (Figure 4c). This suggests increased flexibility of the uL24 tunnel loop located at the mouth of the tunnel exit, consistent with recent RNC

structures reporting similar shifts in uL24 loop upon NC interaction (Tian et al., 2019). In addition to the ribosome tunnel loops at the vestibule, small movements (~1 to 2 Å) were detected in A1321 of H50, A91 nucleotide of H7 in 23S rRNA and A490 nucleotide of H24 in 23S rRNA (Supplementary figure 6), however it is difficult to assess the significance of these displacements since they are below the average level of resolution of our structures. When compared to an empty ribosome structure (not occupied with p-tRNA bound NC), the loops in ribosomal proteins within the tunnel undergo significant shifts: uL23 undergoes a ~ 12 Å and uL24 a ~ 6 Å shift (Figure 4). Similarly, the nucleotides of rRNA domains that interact with FLN6 NC at the vestibule also undergo local movements relative to the empty ribosome: H24 (A490) and H50 (A1321) undergo a shift of ~ 3 Å, and H7 (A91) moving by ~ 2 Å (Supplementary Figure 6). These changes in the structure of these ribosome elements indicate that the ribosome in the presence of NC within the tunnel is accommodating enough to undergo local variations as a result of non-specific interactions with NC, such that it does not stop translation and disrupt the emergence of NC from the tunnel.

To explore what impact of the vestibule environment may have on the NC's trajectory, shifts in the FLN6 NC position were measured by comparing positions of the NC in different states, using state 2 NC as the reference (fixed) point. These shifts were measured at the point of bifurcation occupied by uL23 and H50 rRNA domain, at the start of the tunnel vestibule (Supplementary Figure 8). In FLN5-45 RNC, state 1 NC is shifted by 7 Å with respect to state 2, and state 3 is shifted by 8 Å with respect to state 2. A similar effect is observed in FLN5-47 in which states 1 and 3 are shifted by 5 Å and 7 Å, respectively, relative to state 2 (Supplementary Figure 8). Overall, the shifts of the NC measured between H24 rRNA domain and H7 rRNA domain at the vestibule in both FLN5-45 and FLN5-47 RNCs indicate a range of movement up to ~ 15 Å, which is consistent with the shifts allowed by the 20 Å wide vestibule (Supplementary Figure 8). Altogether, the multiple NC trajectories at the vestibule suggests not only NC mobility but that contacts with the tunnel likely anchor temporary positions of FLN6 NC at the vestibule and therefore induce local conformations. The tunnel vestibule also appears to be actively engaged with NC, affecting NC flexibility and its overall conformation. As a result, movement of FLN6 NC within the vestibule directly affects positions of linked FLN5 NC close to the tunnel exit (as described below).

FLN5 NC is folded close to the ribosome exit tunnel.

Our cryo-EM structures of FLN5-FLN6 RNCs show a distinct bulk of density just outside the vestibule (~ 100 Å from the PTC) which was assigned to the FLN5 domain (Figure 5a) and verified by rigid-body fitting and cross-correlation between the X-ray crystal structure (PDB 1QFH) and the EM density (Figure 5a, Supplementary figure 7a; see methods). The scores of fits (Table 2) indicated that these bulks of densities correspond either to the fully folded or to a folded core of the immunoglobulin domain (Figure 5a).

The structures of RNCs in different states revealed variations in the position of the FLN5 NC close to the ribosomal exit tunnel (Figure 5). In states 1 and 2, FLN5 domains are positioned at ~ 16 to 20 Å away from H24 ribosome domain in FLN5-45 RNC, nearby uL24 ribosome tunnel loop (Figure 5b). By contrast, FLN5 in state 3 of FLN5-45 RNC is positioned ~ 32 Å away from the ribosomal surface (using H24 as a reference point), and located close to the uL29 protein on the opposite site of the ribosome tunnel (State 3, Figure 5b). These variations in the position of FLN5 demonstrate the mobility of FLN5 NC around the ribosome exit surface, which (may be) are affected by FLN6's conformation and the interactions it forms at the vestibule (Figure 3; Supplementary Figure 5).

In FLN5-47 RNC states, FLN5 domain in state 1 is ~ 22 Å away from the tunnel exit in the proximity of H24 domain (Figure 5b). We note that the point of attachment of FLN5 in state 1 of FLN5-47 to the ribosome at H24 rRNA domain is analogous to that of FLN5 observed in states 1 and 2 of FLN5-45 RNC (Figure 5b). The less defined densities of FLN5 in state 2 of FLN5-47 indicate that FLN5 NC is flexible and apparently is shifted by ~ 15 Å away from the ribosomal surface, based on FLN5 domain fitting (Figure 5b). In state 3 of FLN5-47 RNC, FLN5 is located ~ 30 Å away from H24 of the ribosome tunnel (Figure 5c). The FLN5 domain in this state is rotated by ~ 60 degrees towards H59 rRNA domain relative to the FLN5 domain in state 3 of FLN5-45 RNC (state 3, Figure 5b). FLN5 state 3 of FLN5-47 RNC also shows the FLN5 N-terminus interacting with H59 of the 23S rRNA domain, which is located close to the exit of the tunnel (Figure 5b; Supplementary Figure 7c). The contact is possibly mediated by electrostatic interactions of the negatively charged H59 rRNA domain nucleotides and positive charges (corresponding to lysine residues) in the N-terminal loops of FLN5 (Supplementary Figure 7c). We found that FLN5 NC interactions with the ribosome induce a shift of ~ 5 Å in H59 rRNA

loop compared to H59 in empty ribosomes, and a shift of ~ 3 Å in H59 rRNA loop compared with state 2 of FLN5-47 RNC structure (Figure 4d). The shifts of H59 rRNA domain upon NC interaction imply on its possible role as a checkpoint during co-translational folding of an emerging NC, which is consistent with previous observations of interactions between the partially folded NCs on the ribosome and the H59 rRNA domain (Nilsson et al., 2017).

All in all, our results demonstrate that the states of the FLN6 domain within this tandem FLN5-FLN6 NC, arise due to non-specific interactions with the ribosome tunnel. The structures indicate that the nearly folded FLN5 domain can be found in different positions around the tunnel exit during different stages of biosynthesis, whereby its location from the tunnel exit is correlated with NC trajectory adopted within the vestibule. Yet some NC trajectories reflect greater degree of movement within and close to tunnel. State 3 FLN5 NC, specifically in FLN5-47 RNC is mobile enough to reach H59 rRNA domain on the surface of the ribosome and interact non-specifically.

Discussion

In this cryo-EM study we have analysed structures of a tandem of two domains (FLN5-FLN6) as nascent chains on the ribosome with the immunoglobulin domain FLN5 linked to the ribosome by the truncated FLN6 domain. The cryo-EM structures obtained reveal differences in the conformations of RNCs in the two biosynthetic states due to different lengths of the tether: FLN5-45 and FLN5-47. NMR analyses of these two RNCs indicated that emerging FLN5 at the linker of the 45-47 aa has a (nearly) Ig-like fold (Cabrita et al., 2016). The cryo-EM structures reported extend this further by revealing different states adopted by the NC within the tunnel, mediated by the interactions made with the tunnel NC. It appears that NC flexibility at the vestibule is not defined by its sequence and does not affect ribosome's capacity to translate. Instead, this NC flexibility depends on the tunnel dimensions as well as the propensity for any non-specific interactions between the NC and the ribosome tunnel. The interactions between NC and the ribosome also depend on the NC location within the tunnel, more prevalent in the narrow part of the tunnel (upper or central). Our analyses of the structures also show key checkpoints along the ribosome exit tunnel that mediate NC activity within and close to the exit tunnel (Figure 6).

We have captured, for the first time, a multitude of NC states on the ribosome for each of FLN5-45 and FLN5-47, with well-traced density for the NC from the PTC through the ribosomal exit tunnel. The cryo-EM structures reflect the dynamics of the nascent polypeptide within both RNCs showing that the NC to have at least 3 well populated states. In FLN5-45 RNC, the location of the folded FLN5 is better defined near the tunnel exit compared to the slightly longer tether in FLN5-47 RNC structures. The two additional residues linking the folded FLN5 NC domain to the PTC shift the domain slightly further from the ribosome (by ~ 6 Å), enhancing its ability to move nearby the exit tunnel, facilitating temporary points of interaction with a peripheral ribosome region (i.e. the H59 domain of 23S rRNA). An electrostatic interaction between H59 and FLN5 within FLN5-47 RNC appears to stabilise one of the orientations of FLN5 NC.

Local rearrangements within the ribosome exit tunnel observed in our structures further confirm its active role in the presence of NC within the exit tunnel. In particular, the vestibule, where the NC appears most mobile, displayed shifts in both ribosomal RNA and ribosomal proteins lining the tunnel wall. These shifts suggest that without changing the global interaction network within the ribosome, local changes are possible in order to accommodate NC activities within the tunnel. We identified three checkpoints along the ribosome exit tunnel that potentially can modulate NC behaviour inside and outside the tunnel: uL22 at central tunnel, uL23-H50-H24 at the vestibule and H59 outside the tunnel. Published cryo-EM structures of RNCs also implicate uL22 and H59 as main interaction points for an emerging NC, influencing its position within the tunnel and folding (Agirrezabala et al., 2017; Su et al., 2017; Nilsson et al., 2017). The structures further indicate that there is a correlation between NC interactions inside the tunnel affecting positions of the NC domains outside the tunnel. The shorter RNC (FLN5-45) makes the NC less mobile and favouring folding of immunoglobulin domain at exit of the tunnel while the longer NC (FLN5-47) with 2-additional residue shows that the folded immunoglobulin domain outside the exit tunnel is more variable. Overall this increase in the mobility between these states at the point of the folding transition can rationalise the folding of this highly stable domain only occurring at these points during biosynthesis.Comparison of the multiple states described for two RNCs studied shows that in all cases, the FLN6 linker appears to be in a compact state in the vestibule that regulates the position of FLN5 being close to the vestibule, relative to what would be expected for an extended FLN6 linker. The positions occupied by FLN5 NC also appear shorter and closer to

the ribosome exit tunnel than expected for an extended linker (i.e. on average 10-30 Å compared with expected ~ 60 to 70 Å away from the tunnel exit). We suggest that this close proximity of FLN5 to the tunnel exit in both RNCs occurs as a result of FLN6 NC compaction within the vestibule.

The compaction of the tethering linker may explain the observed delay of the folding of FLN5 at lengths 45-47 residues away from the tunnel (Cabrita et al., 2016). Due to FLN6 NC compaction, FLN5 should be able to fold significantly earlier, at shorter linker lengths (Waudby et al., 2018). We can suggest that the compaction of the FLN6 residues within the vestibule may preclude earlier folding since this compaction may compete with FLN5 folding at biosynthesis points. Furthermore, the NMR observations of different complexes with different length of the tether from FLN5-21 to FLN5-42 (Cabrita et al., 2016) indicate that FLN5 remains largely disordered and NMR resonance broadening indicating interactions of FLN5 with the ribosome surface. The FLN6 compaction and the proximity of globular FLN5 to the ribosome observed by cryo-EM indicates that the combination of interactions with ribosome inner surfaces may result in the delayed folding of FLN5 and it's locus, although the folded domain remains close to the vestibule of the ribosome.

The partial compaction observed for the FLN6 NC within the tunnel vestibule further suggests that the vestibule plays an active role during folding by recognising the presence of specific NC amino acids that are involved in transient contacts made with the tunnel. These contacts may stimulate interactions between the NC residues in such way that the NC may be compacted and may allow formation of transient secondary structural elements, particularly at longer. Interesting parallels can also be drawn from recent cryo-EM studies of RNCs of small folded domains on shorter linker lengths: both spectrin (linker length 32aa) (Nilsson et al, 2017) and the immunoglobulin-like protein, I27, (linker length 35aa) (Tian et al, 2018), showing a preference for the orientation shown in our state 3 structure, suggesting that common sites of contact on the ribosome of the newly formed globular state may exist during co-translational folding.

Ackowledgements

This work was supported by the Wellcome Trust (206409/Z/17/Z) to JC. We would like to thank Dr. Dan Clare and Dr. Alistair Seibert at eBIC (Diamond) who assisted in cryo-EM data collection. We thank Dr D. Houldershaw, R. Westlake, and Y. Goudetsidis for computer support throughout the duration of the project. We would also like to thank Prof G. Waksman for productive discussions of the project.

Author Affiliation

E.V.O., L.D.C., and J.C. designed the research. E.V.O. and J.C. supervised the overall project. L.D.C. and A.M.E.C. purified the RNC constructs. A.J. prepared cryo samples, collected data, processed and did structural analysis. A.J., L.D.C, J.C. and E.V.O wrote the manuscript. All authors discussed the results and contributed to the final version.

Three-dimensional cryo-EM density maps of the RNCs complexes have been deposited in the Electron Microscopy Data Bank under the accession numbers EMD-XXXX, EMD-XXXX, EMD-XXXX, EMD-XXXX, EMD-XXXX, EMD-XXXX. Atomic coordinates of the RNCs for each state of the complexes have been deposited in the RCSB Protein Data Bank under the accession codes YYYY, YYYY, YYYY, YYYY, YYYY and YYYY. Correspondence and requests for materials should be addressed to E.V.O. (e.orlova@mail.cryst.bbk.ac.uk) or J.C. (j.christodoulou@ucl.ac.uk)

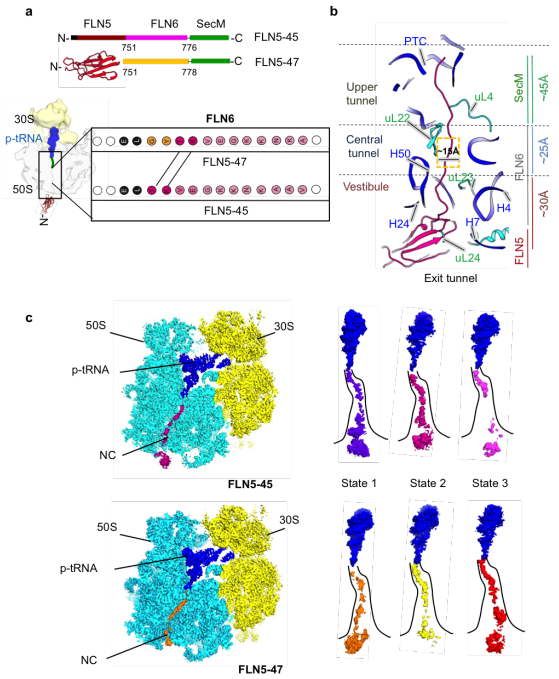

Figure 1. FLN5 RNC complex. a) Schematic diagram of RNC constructs with NC containing sequences of SecM (green), FLN6 (magenta/yellow) and FLN5 (red). The six histidine residues for purification at the N-terminus are shown in black and the two vector residues between DdFLN6 and SecM sequence are shown with a line. The X-ray crystal structure (pdb 1qfh) of FLN5 domain is shown in red. Bottom panel shows a schematic organisation of the FLN5 NC at two linker lengths within the ribosome exit tunnel. Zoom in panel shows the C-terminal sequence of ddFLN6 where the two residues (magenta) differ between FLN5-45 and FLN5-47. Two additional residues in FLN5-47 RNC are shown in yellow. b) Cross-section view of the large subunit of the ribosome, showing ribosome exit tunnel. Ribosomal RNA is shown in dark blue, ribosomal proteins are shown in cyan, FLN6 NC linker and FLN5 Ig domain are shown in magenta. The three main regions of the tunnel are indicated on the left, expected occupancy of FLN5 NC elements are shown on the right. Lengths of upper, central and vestibule regions are indicated on the right. (c) Upper panel shows cryoEM map of FLN5-45 RNC (state 2); 50S shown in blue, 30S in yellow, p-tRNA in dark blue and NC in magenta. Left shown shows the EM density for three NC states of FLN5-45 within the ribosome exit tunnel; state 1 (purple), state 2 (magenta) and state 3 (pink). Bottom left panel shows the cryo-EM map of FLN5-47 RNC (state 2); 50S in light blue, 30S in yellow, p-tRNA in blue and NC in yellow. Bottom right panel shows EM maps of three states of FLN5-47 RNC attached to p-tRNA; state 1 (orange), state 2 (yellow) and state 3 (red).

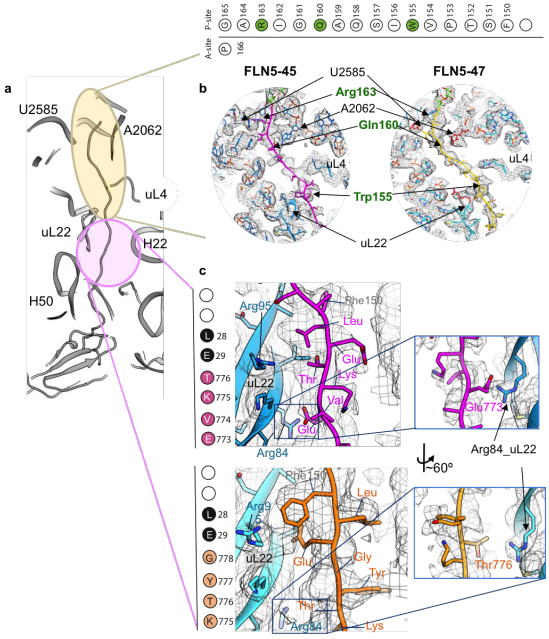

Figure 2. SecM and FLN6 NC within upper and central tunnel. (a) A cross-section view of the exit tunnel, marked with rRNA (dark blue circle) and ribosomal proteins (in cyan circle) regions. Blow-out regions correspond to upper (yellow) and central (pink) tunnel. (b) Upper panel shows sequence of 17 residue SecM NC sequence. C-terminal proline is indicated at the ribosome A-site (not visualised in our maps), linked to Gly-stalled SecM NC. Key interacting residues are coloured in green. Bottom zoom-in panels show the upper tunnel regions from FLN5-45 (state 2 – magenta) and FLN5-47 (state 2 – yellow) RNCs. Ribosomal RNA and proteins are coloured in blue and NC in magenta (+45) and yellow (+47). Nucleotides and proteins residues that interact with SecM NC are shown in red as well as labelled in green. (c) Close-up views of central tunnel in FLN5-45 (state 2 – magenta) and FLN5-47 (state 2 – yellow). Residues of uL22 (blue) and NC are labelled. Left panel shows the residues (single letter acryonym) of FLN6 fitted within the map in FLN5-45 (magenta) and FLN5-47 (yellow). Right panel shows close-up views of interactions between FLN6 NC residues and uL22-Arg84 (blue).

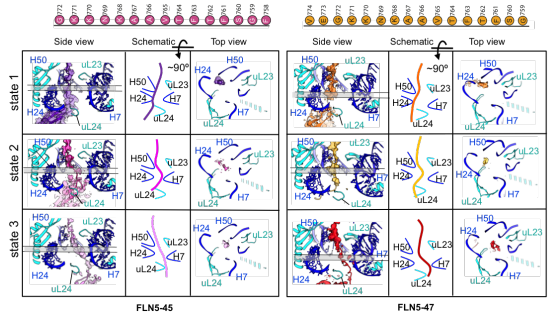

Figure 3. NC trajectories within the vestibule. Top panel shows the FLN6 sequence modelled in each RNC complex (on the left is FLN5-45 - magenta and on the right is FLN5-47 - yellow). Bottom panel shows close up views of the vestibule (side view, schematic and top view panels) of three NC states. Ribosomal RNA is shown in dark blue and proteins in cyan. For FLN5-45 RNC, state 1 is shown in purple, state 2 in magenta and state 3 in pink. For NC states of FLN5-47 RNC: state 1 in orange, state 2 in yellow and state 3 in red.

Materials and Methods

Generation of ribosome-nascent chain complexes (RNCs):. RNC constructs of FLN5-45 and FLN5-47 were derived from a FLN5-110 RNC construct by truncating the C-terminal residues in FLN6 linker sequence, as described previously (Cabrita et al., 2016). The constructs include 17 residues from SecM, two cloning residues, 26/28 residues from FLN6 and the full 105 sequence of FLN5 from ABP120 protein (Figure 1; Cabrita et al., 2016). The FLN5-RNCs were biochemically purified as described in (Cassaignau et al., 2016), though with included minor modifications: Following growth in an un-labelled MDG medium at 37°C, the cells were washed and re-suspended in EM9 medium. RNC expression was induced with 1 mM IPTG at 30°C, and 150 mg/mL rifampicin was added 10 minutes later. The cells were harvested by centrifugation 35 min later. Ribosomal material was recovered from the lysate using a 35 percent (w/v) high salt sucrose cushion prior to purification using a Ni-IDA column. The RNCs were purified further by applying pelleted RNCs to a butyl HP column equilibrated in a high salt buffer (20mM Hepes, 1.5 M NH4SO4, 400mM KOAc, 12mM MgOAc, 2mM BME, 0.1 percent (w/v) protease inhibitors, pH 7.5). RNCs were eluted using a reverse linear ammonium sulfate gradient into a low salt buffer, which lacked ammonium sulfate. RNC integrity was determined using an anti-his western blot against a series of isolated FLN5 standards as described previously (Cabrita et al., 2016).

Sample preparation and Electron Microscopy:. Purified RNCs at ~ 200nM were applied to home-made carbon coated holey-carbon supported grids (C-flat

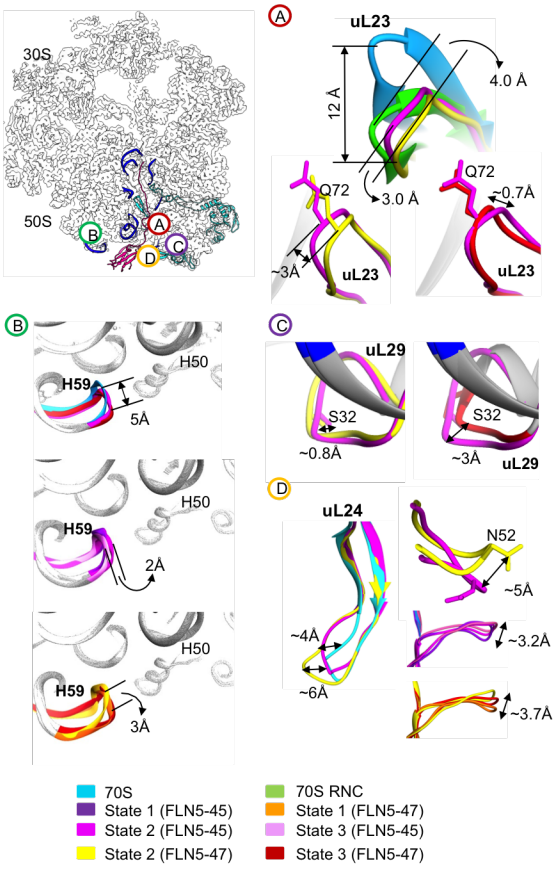

Figure 4. Changes in ribosome tunnel vestibule in FLN5 RNCs. Top right panel shows map of the ribosome in grey, labelled with regions of the exit tunnel (RNA in blue and proteins in cyan). Tunnel regions where structural changes were observed are shown as panels A, B, C and D. Panel A shows changes in uL23, B panel below shows changes in uL29, panel C shows changes in uL24 and panel D indicates changes in ribosomal RNA domain H59.

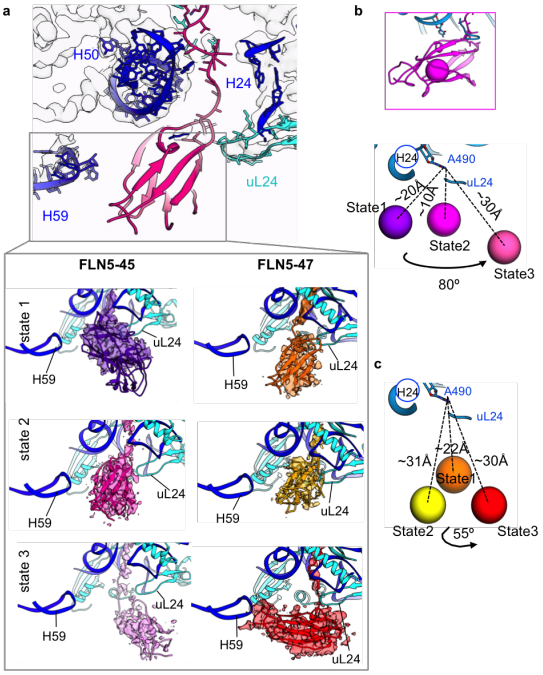

Figure 5. Changes in folded FLN5 NC on the ribosome. a) A zoom in view of the vestibule and tunnel exit where FLN5 NC was modelled. Ribosomal RNA are marked in dark blue, ribosome proteins in cyan and maps of FLN5 states in FLN5-45 and FLN5-47 are indicated in the H59 zoom-in panel as follows; state 1 in purple, state 2 in magenta and state 3 in pink for FLN5-45 states and state 1 in orange, state 2 in yellow and state 3 in red for FLN5-47 states. b) Models of FLN5 grouped in three states (shown as central mass spheres) for FLN5-45 and FLN5-47 RNCs. Insert on the left shows fitted FLN5 immunoglobulin domain and its centre of mass sphere. Right panels show distances measured between the tunnel exit and FLN5 and the degree of rotation of FLN5 between the three states in FLN5-45 and FLN5-47 RNCs. Measured distances of FLN5 position from the tunnel (A490 nucleotide on H24 rRNA domain) are indicated.

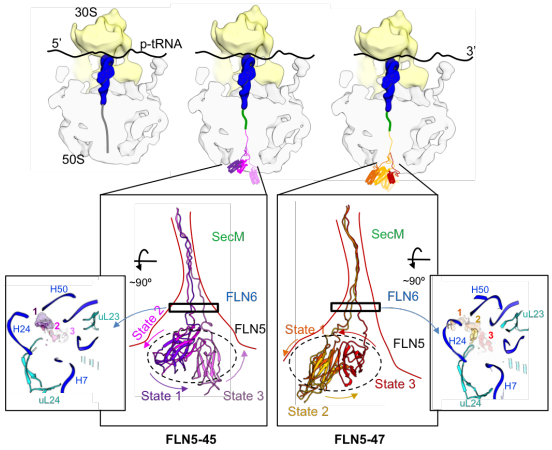

Figure 6. A model for co-translational protein folding. Upper panel shows a schematic diagram of the ribosomes during translation of FLN5 RNC constructs in three steps; step one translating SecM, step two translating FLN5-45 RNC (with its three main states in the zoom-in panel) and step three translating FLN5-47 RNC (three states in the zoom-in panel). Zoom-in panels for each complex indicate the changes observed in FLN6 at the tunnel vestibule (shown from top view, states indicated as 1-3) and changes in FLN5 close to the tunnel exit.

R1.2/1.3, Protochips) vitrified using a Vitrobot Mark IV (ThermoFishcerTM). Data for the FLN5-45 and FLN5-47 RNC complexes were automatically collected on a Titan Krios electron microscope (FEI) operating at 300 kV and equipped with K2 Summit direct electron detector (Gatan Inc.) at the eBIC Diamond light source facility (Harwell Campus, Oxfordshire, UK). The defocus range used was -0.6 to -2.0 µm. Data collection was done using EPU (ThermoFishcerTM). For the FLN5-45 and FLN5-47 RNC samples, movies (45 frames per movie) were collected with a total dose of 45 e-/A2. The pixel size was 1.06 Å/pix. on the sample.

Image-Processing:. Relion 2.0 (R. Fernandez-Leiro and Scheres, 2017) was used for all steps in image processing. For each dataset, movies were aligned using MotionCorr2. CTFFIND4 (Rohou A and Grigorieff N, 2015) was used to determine defocus values. Particles were semi-automatically from aligned micrographs using RELION 'Autopick' programme (R. Fernandez-Leiro and Scheres, 2017). The number of selected particles for the FLN5-45 and FLN5-47 RNC complexes was ~ 400,000 and ~ 384,000 correspondingly. Selected images were extracted within boxes of 400x400 pixels. The extracted particle images were subjected to two-dimensional (2D) classification. Subset selection of 188,830 particles in FLN5-45 RNC and 144,460 in FLN5-47 RNC datasets were refined that gave rise to refined 3.0 Å and 2.8 Å maps respectively. The cleaned

particle sets were then used for analysis of structural heterogeneity by 3D classification in Relion (as shown in Supplementary figure 1). We performed extensive focused 3D classification using RELION around the ribosome exit tunnel (Supplementary figure 1) to resolve several NC states within the tunnel and particles from the selected 3D classes obtained were refined independently. The maps used for structure refinements were sharpened by applying negative B-factors of up to -100 using Relion 2.0 (R. Fernandez-Leiro and Scheres, 2017). FSC was estimated, using gold standard approach. Resolutions are reported using the 0.143 criterion (Table 4).

Atomic Modelling:. The high-resolution cryo-EM structure of the 70S-p-tRNA-Gly complex (PDB 5NP6; Agirrezabala et al., 2017) was used as a starting model for ribosome structure assessments. The PDB model was rigid body fit into sharpened cryo-EM maps in UCSF Chimera (Pettersen et al., 2004) and subsequently refined iteratively using Phenix (Afonine et al., 2018) real space refine and in Coot (Emsley and Cowtan, 2004) for improved structure geometry and overall fit. Refined models were assessed using Molprobity scores (Chen et al., 2010) as well as visual inspection in Coot. For assessment of changes within ribosome tunnel elements, sequence based structure alignments of the fitted ribosome structures were performed in Chimera (Pettersen et al., 2004), and RMSD values were assessed to indicate small or large differences. Electrostatic potential maps for ribosome exit tunnel, FLN6 NC and FLN5 structures were calculated using Chimera (Pettersen et al., 2004), based on calculating surface maps from pdb models and colouring maps based on charge potentials of each residue. Initial SecM NC model was obtained using pdb model 3JBU (Zhang et al., 2015). The model was rigid-body fit into each cryo-EM map in Chimera and then refined manually (residue by residue) in Coot. The SecM NCs were then extended with six to eight C-terminal residues of FLN6 NC and fitted manually in Coot. The differences in positions of the fitted SecM NC in both the FLN5-45 and FLN5-47 RNCs were assessed by RMSD. The NC was traced further by extended the NC model with poly-alanine residues to model ddFLN6 residue positions connected to FLN5. The C-alpha backbone of the entire NC was refined using phenix-real-space refine implemented in Phenix (Afonine et al., 2018). Fitting for FLN5 NC density was done using rigid-body fit in Chimera, using the crystal structure (PDB 1QFH; McCoy et al., 1999). First, the pdb model was manually fitted to reflect C-N terminus vectorial emergence from the ribosome. Step-wise cross-correlations scores were computed using the 'Fit in map' programme at resolutions 10-15 Å, assessing translation and rotation shifts that helped to identify the best fit of model in to map. FLN5 model was subsequently joined with fitted FLN6-SecM model as one NC, for each NC state. Figures were prepared in Chimera (UCSF, Pettersen et al., 2004).

References

Afonine PV, Poon BK, Read RJ, Sobolev OV, Terwilliger TC, Urzhumtsev A, Adams PD. (2018). Real-space refinement in PHENIX for cryo-EM and crystallography. Acta Cryst. D74, 531-544

Agirrezabala X, Samatova E., Klimova M., Zamora M., Gil- Carton D., Rodnina M. V. Valle M. (2017). Ribosome rearrangements at the onset of translational bypassing. Sci Adv, 3 (6), e1700147.

Arenz, S., Bock, L. V., Graf, M., Innis, C. A., Beckmann, R., Grubmüller, H., Vaiana, A. C. Wilson, D. N. (2016). A combined cryo-EM and molecular dynamics approach reveals the mechanism of ErmBL-mediated translation arrest. Nature Commun. 7, 12026.

Bhushan, S., Hoffmann, T., Seidelt, B., Frauenfeld, J., Mielke, T., Berninghausen, O., Wilson, D. N. Beckmann, R. (2011). SecM-stalled ribosomes adopt an altered geometry at the peptidyl transferase center. PLoS Biol. 9 (1), e1000581.

Cabrita, L. D., Cassaignau, A. M. E., Launay, H. M. M., Waudby, C. A., Wlodarski, T., Camilloni, C., Karyadi, M.-E., Robertson, A. L., Wang, X., Wentink, L. S., Goodsell, C. A., Woolhead, M., Vendruscolo, M., Dobson, C. M. Christodoulou, J. (2016). A structural ensemble of a ribosome-nascent chain complex during cotranslational protein folding. Nat Struct. Mol. Biol. 23 (4), 278–285.

Cassaignau, A. M., H. M. Launay, M. E. Karyadi, X. Wang, C. A. Waudby, A., Deckert, A. L. Robertson, J. Christodoulou and L. D. Cabrita (2016). A strategy for co-translational folding studies of ribosome-bound nascent chain complexes using NMR spectroscopy. Nat Protoc 11(8): 1492-1507.

Emsley P, Cowtan K. (2004). Coot: model-building tools for molecular graphics. Acta Cryst. D60, 2126-2132.

Gumbart J, Schreiner E, Wilson DN, Beckmann R,

Schulten K. (2012). Mechanisms of SecM-mediated stalling in the ribosome. Biophys J. 103(2):331-341.

Holtkamp, W., Kokic, G., Jäger, M., Mittelstaet, J., Komar, A. A. Rodnina, M. V. (2015). Co-translational protein folding on the ribosome monitored in real time. Science, 350 (6264), 1104–1107.

Javed A., Cabrita L., Christodoulou J. Orlova V. E. (2017). The ribosome and its role in protein folding: looking through a magnifying glass. Acta Crysta D, 73, 509-521.

Kaiser CM, Goldman DH, Chodera JD, Tinoco I Jr, Bustamante C. (2011). The ribosome modulates nascent protein folding. Science. 334(6063): 1723-1727.

Kosolapov, A. Deutsch, C. (2009). Tertiary interactions within the ribosomal exit tunnel. Nature Struct. Mol. Biol. 16, 405–411.

Liu K, Maciuba K, Kaiser CM. (2019). The Ribosome Cooperates with a Chaperone to Guide Multi-domain Protein Folding. Mol Cell. 74(2):310-319.

Lu J, Hua Z, Kobertz R.W., Deutsch C. (2011). Nascent Peptide Side-chains Induce Rearrangements in Distinct Locations of the Ribosomal Tunnel. J Mol Biol, 411, 499-510.

McCoy A. J., Fucini P., Noegel A. A. Stewart M. (1999). Structural basis for dimerization of the Dictoystelium gelation factor (ABP120) rod. Nat Struct Biol, 6, 836–41.

Nakatogawa H. and Ito K. (2002). The ribosome exit tunnel functions as a discriminating gate. Cell, 108 (5), 629–36.

Netzer, J. W. Hartl, F. U. (1997).Recombination of protein domains facilitated by co-translational folding in eukaryotes. Nature, 388 (6640), 343–349.

Nilsson, O. B., Hedman, R., Marino, J., Wickles, S., Bischoff, S., Johansson, M., Müller-Lucks, A., Trovato, F., Puglisi, J. D., O'Brien, E. P., Beckmann, R. von Heijne, G. (2015). Cotranslation Protein Folding inside the Ribosome Exit Tunnel. Cell. Rep. 12, 1533–1540.

Nilsson, O. B., Nickson, A. A., Hollins, J. J., Wickles, S., Steward, A., Beckmann, R., von Heijne, G. Clarke, J. (2017).Cotranslational folding of spectrin domains via partially structured states. Nature Struct. Mol. Biol. 24, 221–225.

Peterson JH, Woolhead CA, Bernstein HD. (2010). The conformation of a nascent polypeptide inside the ribosome tunnel affects protein targeting and protein folding. Mol. Microbiol. 78(1):203-217.

Pettersen EF, Goddard TD, Huang CC, Couch GS, Greenblatt DM, Meng EC, Ferrin TE. (2004). UCSF Chimera – A visualization system for exploratory research and analysis. J Comput Chem 25 (13):1605-12.

R. Fernandez-Leiro Scheres S.H.W. (2017).A pipeline approach to single-particle processing in RELION. Acta Cryst. D73, 496-502

Rohou, A, Grigorieff N. (2015).CTFFIND4: Fast and accurate defocus estimation from electron micrographs. J Struct Biol. 192:216–221.

Samelson AJ, Bolin E, Costello SM, Sharma AK, O'Brien EP, Marqusee S. (2018). Kinetic and structural comparison of a protein's cotranslational folding and refolding pathways. Sci Adv. Vol 4. (5).

Su T., Cheng J., Sohmen D., Hedman R., Berninghausen O., von Heijne G., Wilson D. N. Beckmann R. (2017). The force-sensing peptide VemP employs extreme compaction and secondary structure formation to induce ribosomal stalling. Elife, 6.

Thommen M., HoltKamp W. Rodnina V. M. (2017). Co-translational protein folding: progress and methods. Curr Opin Struct Biol, 42, 83-89.

Tian P, Steward A, Kudva R, Su T, Shilling J P, Nickson A A, Hollins J J, Beckmann R, Heijne von G, Clarke J, Best R (2018). The Folding Pathway of an Ig Domain is Conserved On and Off the Ribosome. PNAS. 115(48); E11284-E11293.

Woolhead CA, McCormick PJ, Johnson AE. (2004). Nascent membrane and secretory proteins differ in FRET-detected folding far inside the ribosome and in their exposure to ribosome proteins. Cell. 116(5):725-736.

Zhang, J., Pan X., Yan K., Sun S., Gao N. Sui S. F. (2015). Mechanisms of ribosome stalling by SecM at

multiple elongation steps. Elife, 4, e09684

Tables

	State1	State2	State3
	FLN5-45		
NC trajectory	H24 rRNA	Middle	H7 rRNA
Number of particles in 3D	5,410	44,732	7,824
	FLN5-47		
NC trajectory	H24 rRNA	Middle	H7 rRNA
Number of particles in 3D	5,712	30,047	20,653

Table 1. NC states identified in FLN5 RNC complexes.

	State1	State2	State3
	FLN5-45		
CC-fit Model to EM map	0.72	0.78	55
	FLN5-47		
CC-fit Model to EM map	0.75	0.45	0.76

Table 2. Fitting scores for FLN5 in EM maps of FLN5-45 and FLN5-47 RNCs.

	FLN5-45-1	FLN5-45-2	FLN5-45-3	FLN5-47-1	FLN5-47-2	FLN5-47-3
EMDB	XXXX	XXXX	XXXX	XXXX	XXXX	XXXX
PDB	YYYY	YYYY	YYYY	YYYY	YYYY	YYYY
Microscope	Titan Krios (300kV)					
Pixel size (Å/pix.)	1.06	1.06	1.06	1.06	1.06	1.06
Electron Dose (e-/A2)	40			40		
Defocus range (μm)	(-0.8 to -2.0)			(-0.6 to -2.0)		
3D refinement						
Software	Relion 2.0					
Number of Particles	5,410	44,732	7,824	5,712	30,047	20,653
Resolution (Å, 0.143 criterion)	3.8	3.1	3.6	3.4	2.9	3
Resolution (Å, 0.5 criterion)	6.6	3.7	5.5	6.3	3.5	3.8
Sharpening B factor (Å2)	-53	-59	-49	-63	-48	-42
Model Refinement & Validation						
Refinement software	Phenix & Coot					
All-atom Clashscore	8.89	4.72	7.35	4.89	6.15	3.9
Ramachandran						
Outliers	0.23	0.37	0.4	0.63	0.29	0.31
Favoured %	87.9	90.22	87.91	90.85	87.08	91.02
Allowed %	11.8	9.41	11.69	8.52	12.64	8.66

Table 3. Cryo-EM structure refinement of FLN5-RNCs.

Supplementary Figures

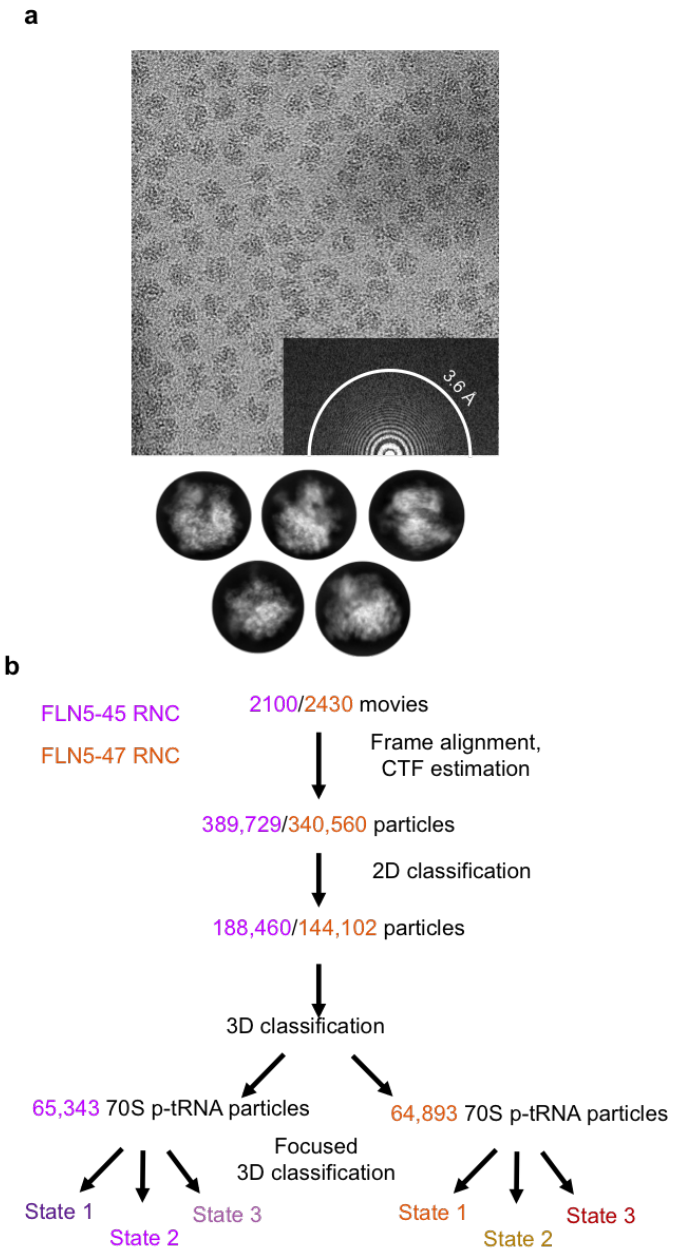

Supp.Fig.1

Changes in ribosome tunnel vestibule in FLN5 RNCs. Top right panel shows map of the ribosome in grey, labelled with regions of the exit tunnel (RNA in blue and proteins in cyan). Tunnel regions where structural changes were observed are shown as panels A, B, C and D. Panel A shows changes in uL23, B panel below shows changes in uL29, panel C shows changes in uL24 and panel D indicates changes in ribosomal RNA domain H59.

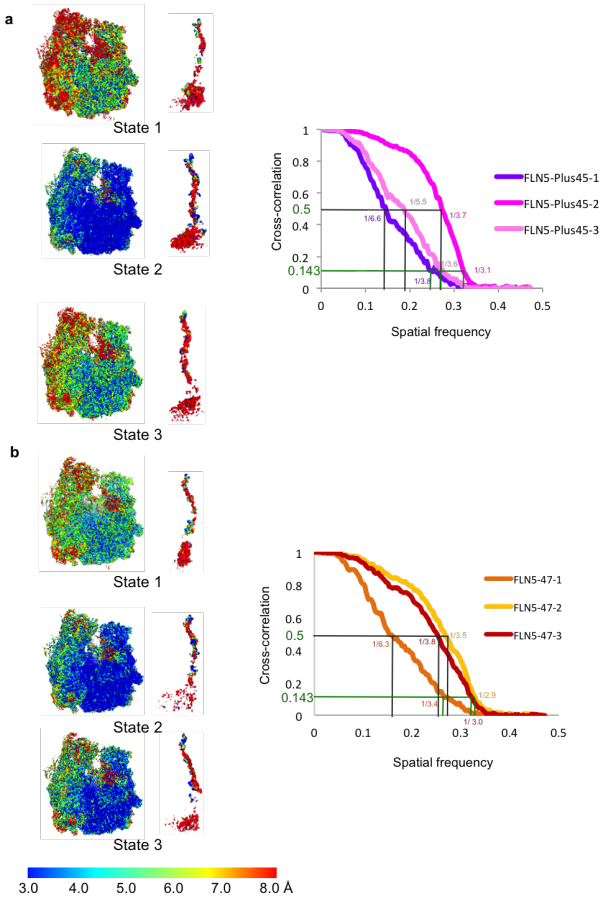

Supp.Fig.2

Local resolution and FSC of FLN5-RNCs. Right panel shows local resolution maps of FLN5-45 (a) and FLN5-47 (b) RNC states, coloured according to the local resolution across the map. For each RNC state, Fourier Shell-correlation curves are indicated (left panel), with resolutions computed at both 0.5 and 0.143 FSC criterion.

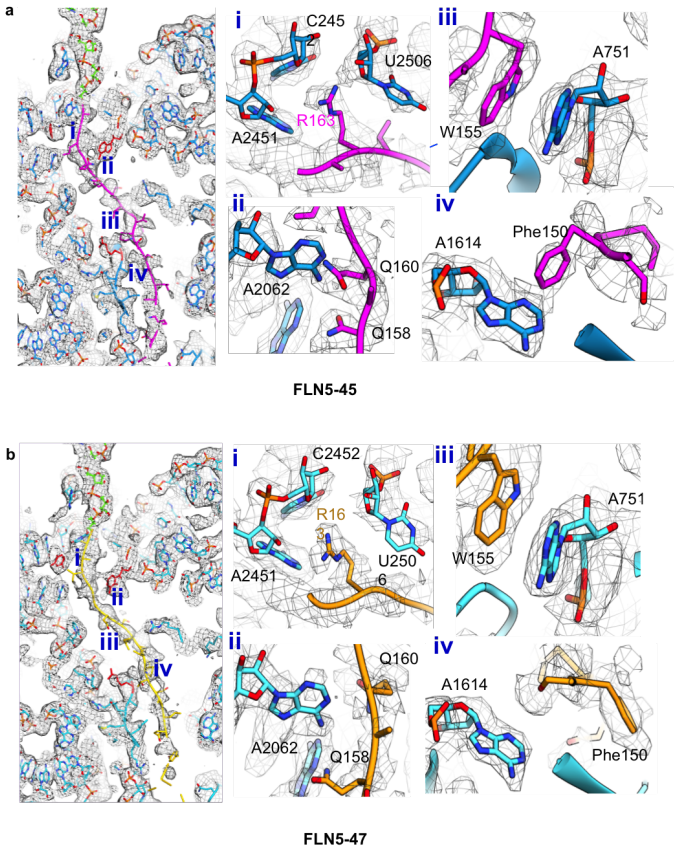

Supp.Fig.3

SecM interactions with the ribosome exit tunnel in FLN5-45 and FLN5-47 RNC complex. a) Cross-section view inside the exit tunnel shows exit tunnel elements and fitted SecM NC in state 2 (in magenta) of FLN-45 RNC complex. Map is visualised at sigma value of 1.5. Zoom-in panels i-iv highlight the interaction points between the SecM NC and the ribosome elements (in blue) lining the upper and central tunnel regions. b) Cross-section shows exit tunnel elements and fitted SecM NC in state 2 (in yellow) map of FLN5-47 RNC complex. Map is visualised at sigma value of 1.5. Zoom-in panels i-v highlight the interaction points between the SecM NC and the ribosome elements (in blue) lining the upper and central tunnel regions.

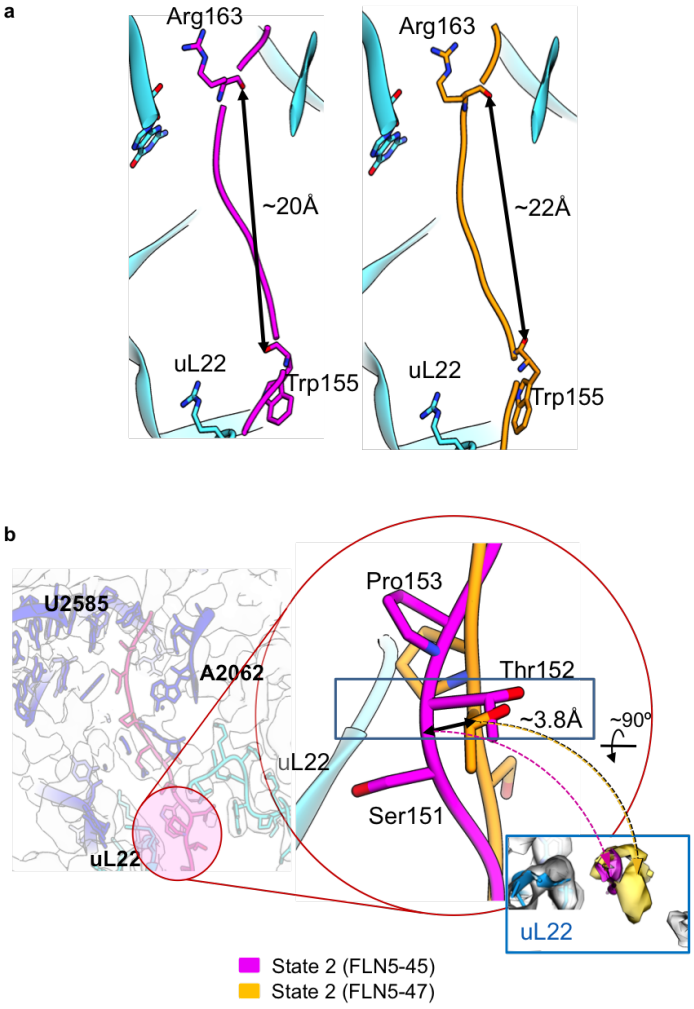

Supp.Fig.4

Changes in SecM NC in FLN5 RNC. a) SecM NC states 2 in FLN5-45 (magenta) and FLN5-47 (yellow) RNCs are shown with measured distances of the 10 residues (from Arg163 to Trp155) at the upper tunnel, indicating NC compaction. Ribosome tunnel elements are coloured in blue. b) Cross-section view of upper tunnel with labelled areas (in green) where SecM interacts. A zoom in panel (circled in red) indicates the N-terminal segment of SecM that undergoes a shift of 3.8 Å between FLN5-45 and FLN5-47 RNCs state 2.

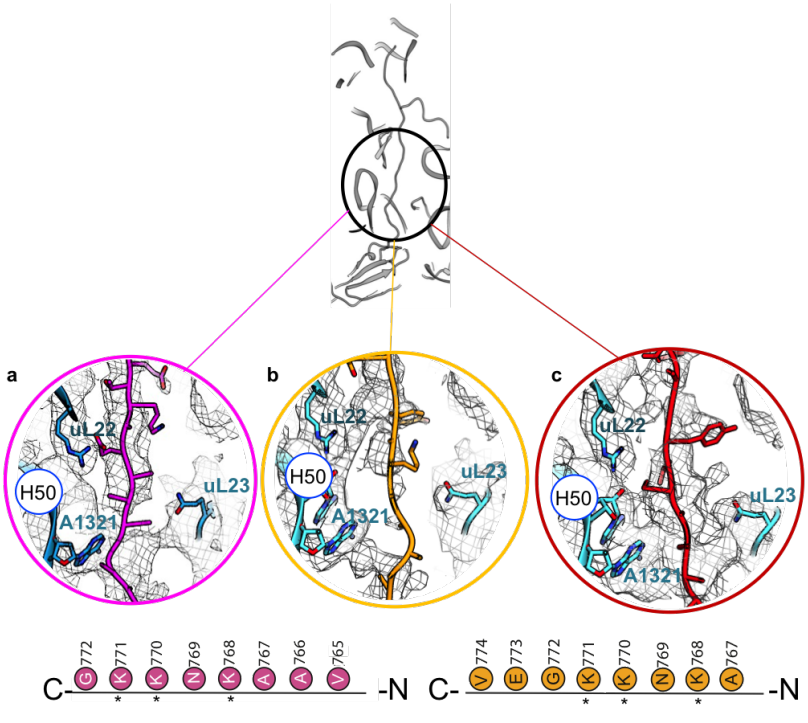

Supp.Fig.5

Bifurcation point of FLN6 NC at the ribosome exit tunnel. Top panel shows the highlighted region of the ribosome exit tunnel (circle in black) occupied by nucleotides of H50 and residues of uL23. Zoom out panels a-c below show EM map and fitted model of ribosome and NC where interaction points are observed in state 2 of FLN5-45 (in magenta), state 2 of FLN5-47 (yellow) and state 3 of FLN5-47 (red) respectively. Bottom panel shows sequences from FLN6 linker corresponding to the NC shown in panels a-c. Interactions points between ribosome tunnel and FLN6 NC (a-c) are indicated as asterisk.

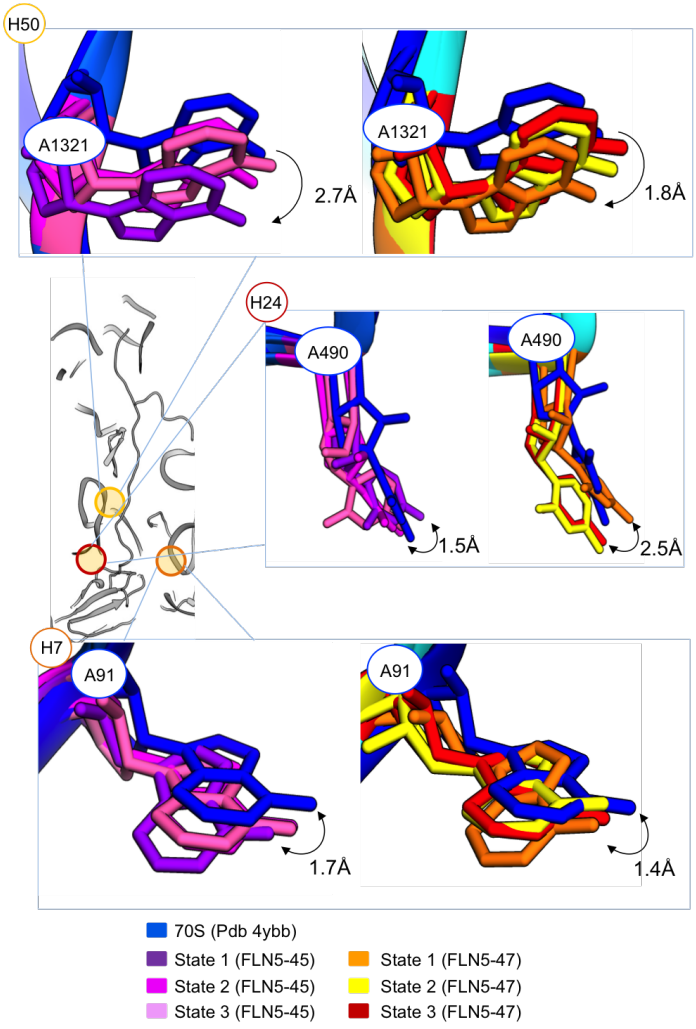

Supp.Fig.6

Changes in ribosomal RNA at the tunnel vestibule in FLN5 RNCs. Middle left panel shows exit tunnel cross-section with marked areas where changes were analysed. Top panel (H50) shows changes in H50 rRNA at A1321 nucleotide position from 70S (blue) and FLN5-45 states (left panel) and FLN5-47 states (right panel). Measured distances are labelled. Middle panel (H24) shows changes in H24 rRNA at A490 nucleotide from 70S (blue) and FLN5-45 states (left panel) and FLN5-47 states (right panel). Bottom panel (H7) shows changes in H7 A91 nucleotide from 70S (blue) and FLN5-45 states (left panel) and ddFLN5-47 states (right panel).

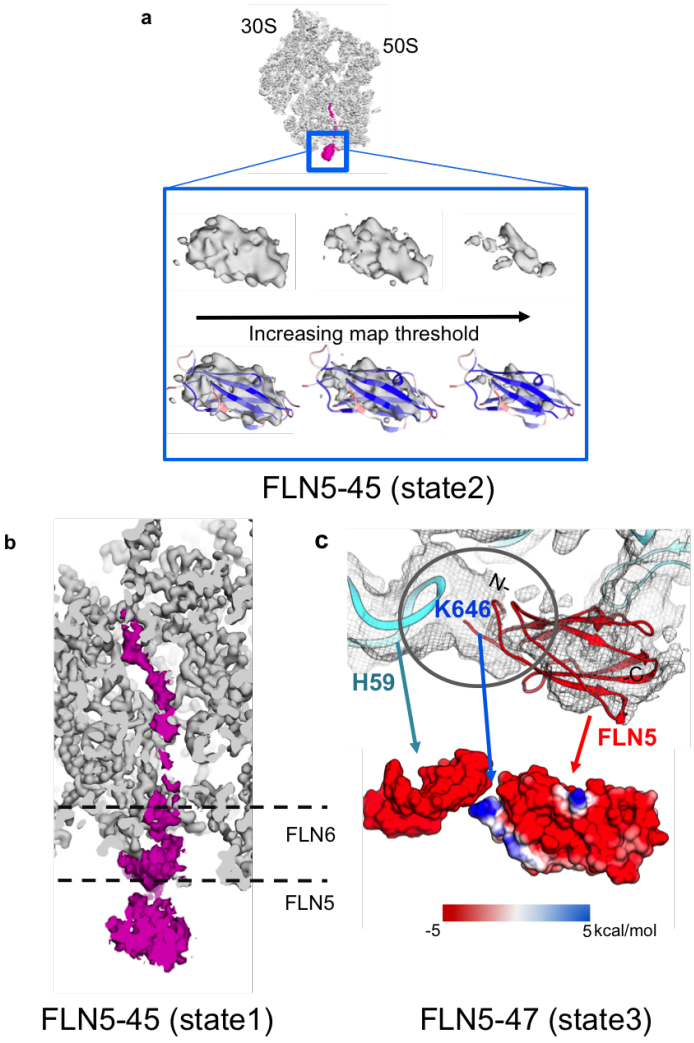

Supp.Fig.7

NC activities within the ribosome exit tunnel. a) Panel a shows the EM map of FLN5-45 RNC state 2 map, with NC density coloured in magenta. A zoom-in panel (in blue) shows segmented NC density of FLN5 NC in FLN5-45 state 2, visualised at three map threshold values (top panel), overlaid with fitted FLN5 model (bottom panel – coloured according to RMSD values computed between NMR and X-ray structures). Panel b shows cross-section of exit tunnel in the cryo-EM map of FLN5-45 RNC state 1, with ribosome in grey and segmented NC in purple. The map is visualised at sigma value 1, showing FLN6 compaction, attached to a globular FLN5 NC outside the tunnel. FLN6 and FLN5 areas are marked as dashed lines. Panel c shows a close-up view into FLN5-47 RNC states 3 at the interaction point of H59 rRNA. Map (in grey mesh) is gaussian filtered (1.06 pix) for purposes of visualisation. Fitted FLN5 domain is shown in red, H59 rRNA domain in blue. Bottom panel shows the electrostatic surface maps for H59 rRNA and FLN5 NC (red – negatively charged, blue – positively charged).

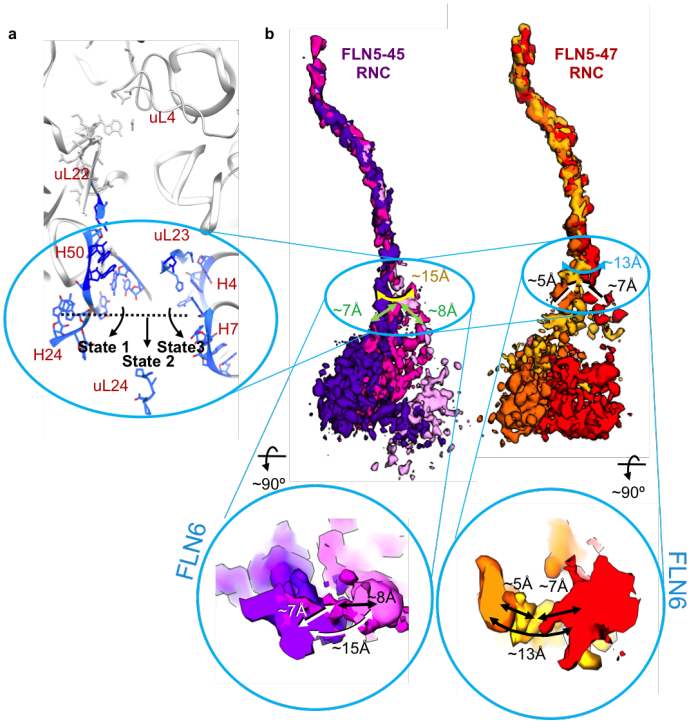

Supp.Fig.8

Multiple states of FLN5 NC on the ribosome. (a) Panel shows cross-section of ribosome exit tunnel and the bifurcation of NC states at the tunnel vestibule. (B) An overlay of NC EM maps of states 1-3 in FLN5-45 (left panel) and states 1-3 in FLN5-47 (right panel) RNCs. Relative shifts between each state is indicated: shifts between state 1-2 and state 3-2 is indicated by green arrows (FLN5-45) and black arrows (FLN5-47) whilst the shift between state 1 and 3 is indicated by yellow arrow (FLN5-45) and cyan arrow (FLN5-47 RNC). Bottom panels show a close of the vestibule area (top view) of overlay of 3 states and relative shifts in FLN5-45 and FLN5-47 RNCs.